Uniaxial deformation of 2D polydisperse froths

1999 J. Phys.: Condens. Matter 11 7947

(http://iopscience.iop.org/0953-8984/11/40/318)

J. Phys.: Condens. Matter **11** (1999) 7947–7957. Printed in the UK PII: S0953-8984(99)04513-0

Uniaxial deformation of 2D polydisperse froths

M A Fortes and M Emília Rosa

Departamento de Engenharia de Materiais, Instituto Superior Técnico, Lisboa, Portugal

Received 24 May 1999, in final form 21 July 1999

Abstract. We have studied experimentally the uniaxial deformation of polydisperse 2D monolayer liquid foams. The main topics addressed are: (i) the frequency of T1 events; (ii) the trajectories of individual bubbles; (iii) the variation of topological disorder; (iv) the change in foam energy (length of films) and in the orientation of the films. We compare the results for polydisperse froths with those previously reported for a honeycomb froth.

1. Introduction

This paper describes and discusses results of an experimental study of the uniaxial deformation (tension/compression) of 2D disordered froths containing a large number of bubbles. In another paper [1] we will report experiments on froths consisting of a few bubbles, for which we calculated the foam energy exactly.

Recent reviews of foam deformation include Kraynik [2] and Weaire and Fortes [3]. Most of our understanding of foam deformation derives from computer simulations (e.g. [4–7]) and a small number of experiments (e.g. [1, 8, 9]).

Two processes contribute to the deformation of a 2D dry froth, that is, one with a small liquid fraction. At sufficiently small strains, films can stretch at constant topology, in a linear elastic (reversible) deformation. In this regime, the foam energy varies parabolically with strain, with a Young's modulus Y given by (e.g. [10, 11])

$$Y = \lambda \frac{\gamma}{a} \tag{1}$$

where γ is the film tension, a is a characteristic linear dimension of the bubbles and λ is a constant that depends on the choice of a and on the geometry and topology of the foam. For a honeycomb froth $\lambda = 1/(2\sqrt{3})$, if a is set to the edge length of the hexagonal bubbles [9]. If deformation occurs at constant bubble size, as in the experiments that we report in which the foam behaves as incompressible, the Poisson ratio is $\nu = 1$ in 2D. This implies that a strain, ε, in one direction causes a strain, $-\varepsilon$, in the perpendicular direction. Since a foam with random oriented films is isotropic, the elastic behaviour of an (isotropic) incompressible foam is then completely defined by a single elastic property, for example, Y.

At larger strains topology changes in the foam, through neighbour switching events (T1 events), see figure 1(a). The length of a particular edge (film) AB, separating cells A and B, reduces to zero and the two cells A and B sharing that edge lose adjacency while the cells C and D, originally at the vertices of AB, become adjacent [12]. For bubbles adjacent to walls, the corresponding transformation is the T1′ transformation, shown in figure 1(b) [13]. A new bubble becomes adjacent to a wall (and loses adjacency in the reverse T1′ transformation).

0953-8984/99/407947+11$30.00

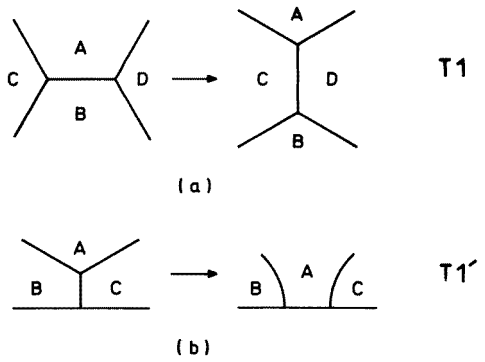

Figure 1. (a) The T1 or neighbour switching transformation: second neighbour cells C and D become adjacent while A and B lose adjacency. (b) The T1′ transformation of three cells near a wall: cell A changes its neighbour relation with the wall.

T1 and T1′ events decrease the free energy (i.e. the total length of the bubble films) under a fixed imposed strain and frequently propagate to adjacent bubbles leading to an avalanche of successive T1 events [1, 6, 14]. T1 avalanches have also been observed in Langmuir monolayer foams [15].

In an ordered honeycomb froth these avalanches result from the glide of a 5/7 pair (pair of adjacent bubbles with five and seven sides) which is, in fact, a dislocation with a unit Burgers vector [9]. The dislocations nucleate at the free surface of the honeycomb and then glide (in an avalanche of T1 events), reflecting at the walls confining the foam sample (T1′ events). They eventually leave the foam at its free surface, and the perfect honeycomb reappears.

In disordered froths, this description of T1 events and their avalanches in terms of dislocation glide does not apply, because there is no reference configuration of the foam in relation to which a dislocation defect can be defined.

Such irreversible deformation based on T1 events is also relevant to superplasticity (e.g. [15, 16]). A superplastic material can be deformed by this mechanism to very large strains (up to several thousand per cent) in tension. The grains repeatedly change neighbours and remain approximately equiaxed.

Although we have a general picture of deformation by T1 events, a number of related topics still need clarification. We undertook experiments on 2D foam deformation to improve characterization and understanding of general deformation problems. We addressed the following:

(1) The relation between the number of T1 events per bubble and the strain.

(2) The shuffling deformation causes in the arrangement of the bubbles and, in particular, the trajectories of individual bubbles through a sample under deformation.

(3) The evolution with deformation of the topological disorder of the foam, measured by the second moment, μ_2, of the distribution of the number of sides, n.

(4) The change in energy (length of films) caused by film stretching and by T1 events.

(5) The change of orientation (rotation) of the films induced by uniaxial strain.

Our study applies to fairly dry foams. We made no attempt to investigate the effect of the liquid fraction in the foam.

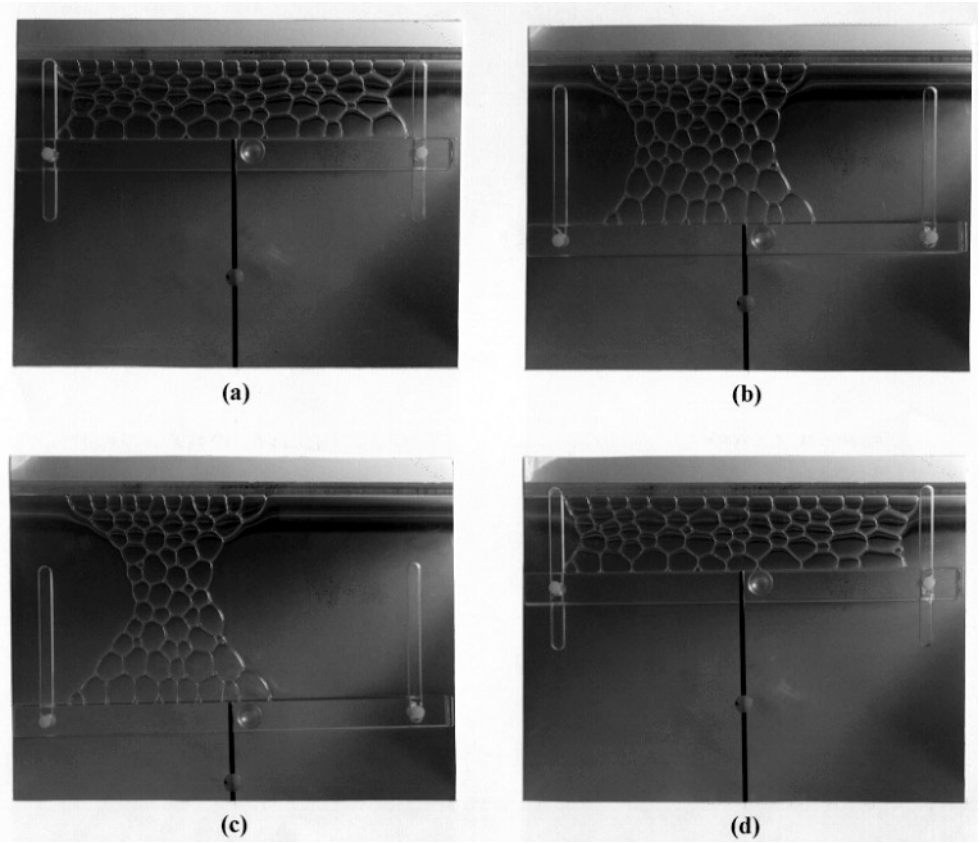

Figure 2. Sequence of foam configurations in uniaxial deformation for the following values of the bar separation, w: (a) w_0(initial state) $= 16$ mm; (b) $w = 32$ mm; (c) $w = 42$ mm; (d) $w = 15$ mm showing the evolution of the necked configuration.

2. Experiment

The foams used in the experiments were polydisperse monolayer foams [1, 9, 17] which consist of a single layer of bubbles of different sizes sandwiched between the originally free surface of the liquid forming the films and a parallel glass plate at a typical separation of 5 mm. The foams are essentially 2D and are confined by two parallel bars in their plane (see figure 2), one of which can be displaced to change the width w of the sample. In the experiments reported here, the number of bubbles in a sample was typically 100, with an average area per bubble around 10 mm^2. The number of bubbles did not change in an experiment. Deformation also occured at constant bubble size (negligible coarsening).

We define the strain ε as:

$$\varepsilon = \ln \frac{w}{w_0} \tag{2}$$

where w_0 is the width of the foam in a reference state (usually the initial state of the as-prepared foam) and w its current width, which is changed by displacing the moving bar. We measured the width w with a ruler (precision of 0.5 mm). The amount of deformation can also be specified in terms of a nominal strain, $\varepsilon_n = (w - w_0)/w_0$. For small strains, $\varepsilon_n \simeq \varepsilon$. A strain ε in one direction of a 2D incompressible medium originates a strain $-\varepsilon$, in the direction

perpendicular to it. The corresponding nominal strains are, however, not symmetrical. It is therefore more convenient to use the logarithmic strain ε.

The foams were photographed for measurement of the relevant quantities. The total length of films was measured by image analysis methods in the skeletized froth. We also measured, by hand, the number, P, of films intersected per unit length of straight lines parallel ($P_{\parallel}$) and perpendicular ($P_{\perp}$) to the direction of displacement of the moving bar, using a set of parallel equidistant lines.

3. Results

3.1. General observations

As the bar moves to change the separation w, T1 events are observed, frequently in the form of avalanches. In addition to the T1 events the foam also deforms by changing the length and orientation of films. The T1 avalanches propagate along an irregular path at a variable angle to the confining bars and are reflected when they reach a bar, as do glide dislocations in a honeycomb froth [9]. The T1 events may occur at the periphery of the foam or inside it; avalanches also initiate either at the surface or in the bulk. This is distinct from the behaviour of honeycombs in which all T1 processes initiate at the free surface [9].

Necking at the centre of the foam samples occurs both in tension and compression, as in the honeycombs. In tension, deformation (i.e. the T1 events) then concentrates in the more and more pronounced neck. Figures 2(a)–2(d) show necking in a 2D disordered foam deformed in tension. If we compress the necked configuration obtained in tension, the neck becomes less sharp but does not disappear (figure 2(d)). Why necking occurs is not clear, but, as in the honeycomb [9], a necked configuration has smaller energy than one with fewer bubbles at the bars, because of the positive binding energy of the bubbles to the bars.

3.2. Frequency of T1 events

We counted the total number of T1 events (isolated and in avalanches) by inspecting the successive configurations of a foam under tension. Figure 3 shows the total (accumulated) number s of T1 (and T1′) events divided by the total number N of bubbles in a foam sample (foam sample 1) as a function of ε. The relation is linear, with

$$\frac{s}{N} = k\varepsilon \tag{3}$$

where k is a constant. In figure 3 the value of $k = 1.31$. A similar linear relation was found in experiments with monolayer Langmuir foams [15] with $k = 0.15$, and also in simulations with $k = 0.15$ [7] and $k = 0.5$ [18], independent of strain rate. A considerable rate effect on k was found in Potts model simulations [7].

We can explain the linear dependence (equation (3)) as follows. As for dislocation glide, a T1 avalanche can be regarded as contributing to the global elongation (strain) with a unit glide displacement b which can be taken as an average separation between the centres of adjacent bubbles. Consider the deformation of a foam sample of width w and length L (parallel to the confining bars). When a T1 avalanche ('dislocation') traverses the foam (eventually reflecting at the bars), the width w increases by $b \sin\alpha$, where $\sin\alpha$ is the average sine of the angle between the avalanche path (glide direction) and the bars. The number, s, of bubbles traversed by the 'dislocation' is the number of bubbles in the glide direction, of total length $L/\cos\alpha$. This number, $s = L/(b\cos\alpha)$, is also the number of T1 events that occurred when the 'dislocation' traversed the entire specimen, producing a strain increment $\Delta\varepsilon = b\sin\alpha/w$.

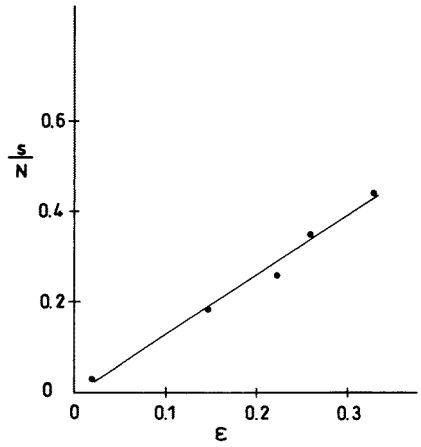

Figure 3. Number, s/N, of T1 and T1′ events per cell that occur in tensile deformation to a strain ε. N is the total number of bubbles in the sample. The best fit straight line is drawn.

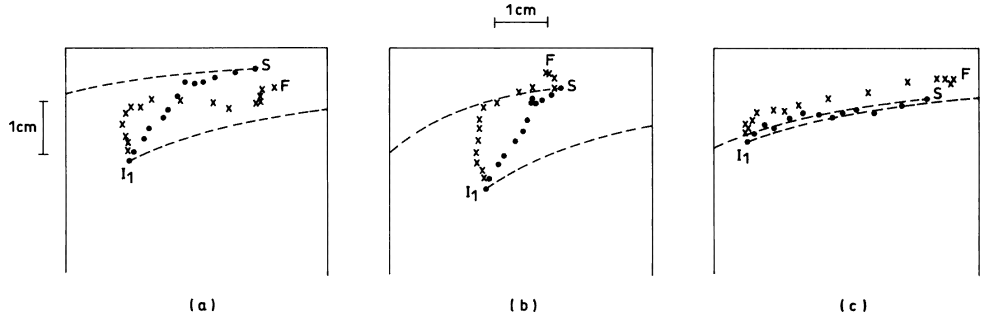

Figure 4. The observed path of individual bubbles in a tension/compression cycle. The upper straight line represents the fixed bar. The initial position of a bubble is S. After tension to $\varepsilon = +1.1$ the bubble is at I_1. After compression to $\varepsilon = -0.4$, the bubble reaches F. Successive locations in tension are (●) and in compression are (×). The dashed lines are calculated trajectories from S and I for homogeneous deformation of an incompressible medium.

Equation (3) then follows, with $k = 2A/(b^2 \sin 2\alpha)$, since the total number of bubbles in the foam is $N = Lw/A$, where A is the area per bubble, with $A \simeq b^2$. For a honeycomb (edge length a) we have: $\alpha = 60^\circ$, $b = a\sqrt{3}$ and $A = (3\sqrt{3}/2)a^2$; so $k = 2$, slightly larger than the experimental value for the polydisperse foam, possibly due to the relatively large α for the honeycomb.

3.3. Shuffling of bubbles

If we identify the individual bubbles (not difficult in a polydisperse froth) we can follow their location as a function of ε. Figure 4 gives examples of bubble trajectories in tension/compression cycles. The trajectories are irregular and, in general, irreversible in a cycle. In figure 4 we compare the trajectories with those (dashed lines) that would result if deformation were homogeneous (see the appendix). In general, the actual trajectories deviate considerably from those for homogeneous deformation as in figures 4(a) and 4(b), but there

are exceptions (figure 4(c)). In narrow samples (few bubbles across the two bars) shuffling may transfer bubbles from adjacency to one bar to adjacency to the other.

When we cyclically deform the foam between two strains, ε_1 and ε_2, its configuration at the extreme strains varies from cycle to cycle. Since the number of configurations of the bubbles for a given ε (i.e. a given separation w) is finite, configurations will, in principle, repeat over a sufficiently large number of cycles, but for many bubbles this number may be too large to observe repetition.

3.4. Variation of topological disorder

With each bubble in a foam we associate a number n, equal to its number of sides (or films) for bulk bubbles. For bubbles at the bars or at the free surface, n is the number of neighbours (films) plus 2 (or plus 3, for the few surface bubbles adjacent to the bars). The average value of n for all cells varied between 5.94 and 5.99, below the ideal value, 6. We calculated the second moment, μ_2, defined as:

$$\mu_2 = \langle (n-6)^2 \rangle. \tag{4}$$

Figure 5 shows plots of μ_2 as a function of ε for two foam samples (samples 1 and 2). The initial μ_2 is larger for sample 1 ($\mu_2^0 = 0.9$ compared with $\mu_2^0 = 0.4$ for sample 2). The samples experienced different tension/compression cycles (sample 1 was first deformed in tension, while sample 2 was first deformed in compression). In both samples, μ_2 fluctuates with ε, but tends to increase in tension and decrease in compression. While μ_2 shows a small change with ε in sample 1 (larger μ_2), a clear increase in μ_2 after one cycle occurs for sample 2.

For uniaxial deformation of a honeycomb froth, the bubbles remain hexagonal and $\mu_2 = 0$, independent of ε. Deformation induced ordering of a disordered foam [4], with a consequent decrease in μ_2, was not experimentally observed. Indeed, calculations by Godrèche *et al* [19] show that random T1 operations, successively applied to a trivalent network, induce a stationary value of $\mu_2 = 4.2$, far greater than the observed μ_2 in the deformed disordered froths, indicating that the edges AB involved in the T1 operations are not 'chosen' at random. On the other hand, if the edge AB (figure 1(a)) is randomly chosen in a network with no correlation between the n values of adjacent cells (i.e. a gas network [20]), μ_2 increases on average by $2/N$ per T1 event, where N is the total number of cells. This is because the change in $\sum(n-6)^2$ due to the switching in figure 1(a) is $2(c+d-a-b)+2$, where a is the number of sides of cell A, etc (see figure 1(a)). We must then conclude that the 'switching edges' AB must connect predominantly cells A and B with many sides, such that μ_2 may even decrease in a T1 event. This correlation will occur if the edges separating cells with many sides are shorter on average, and therefore more prone to switching. This topic needs further investigation.

3.5. Total length of films

Figure 6 shows a plot of L_S (the total length of films per unit area) of sample 2 as a function of strain ε, over a large interval of ε, including two successive tension/compression cycles. The length of films tends to increase in tension, $\mathrm{d}L_S/\mathrm{d}\varepsilon > 0$, and decrease in compression, with L_S approximately returning to its initial value after one cycle. On average, $L_S(\varepsilon)$ is nearly linear, with L_S increasing with ε.

The total force required to deform the foam, per unit thickness of the monolayer, is:

$$F = \frac{A\gamma}{w}\frac{\mathrm{d}L_S}{\mathrm{d}\varepsilon} \tag{5}$$

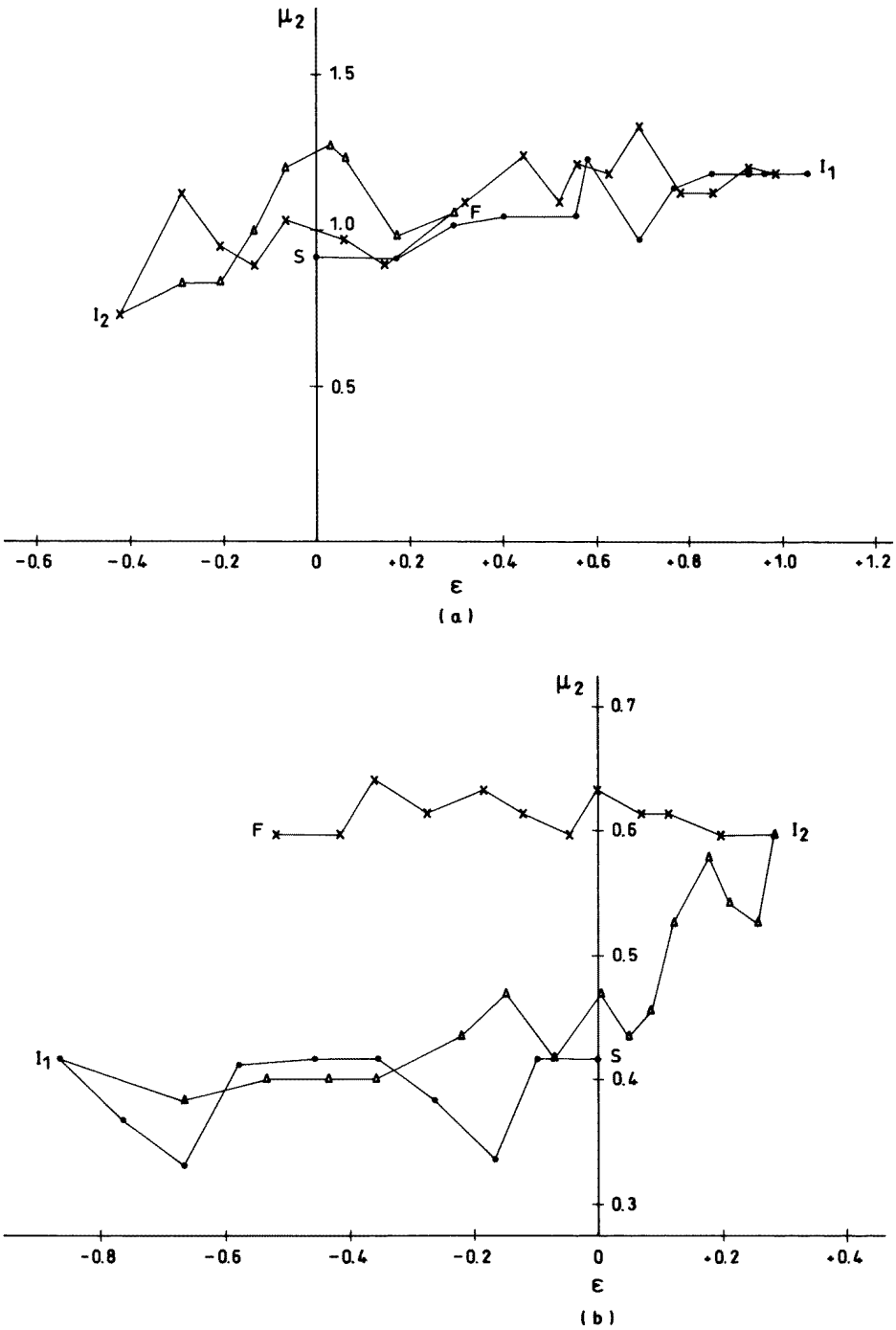

Figure 5. Variation of the second moment, μ_2, with ε in a sequence of tension/compression to the initial w_0 followed by further compression/tension. S is the starting value and F is the final value after the full cycle. I_1 and I_2 are the values at the end of the half-cycles. (a) Foam sample 1 (initial $\mu_2 = 0.9$); (b) foam sample 2 (initial $\mu_2 = 0.4$). Different symbols are used for the experimental points in different cycles.

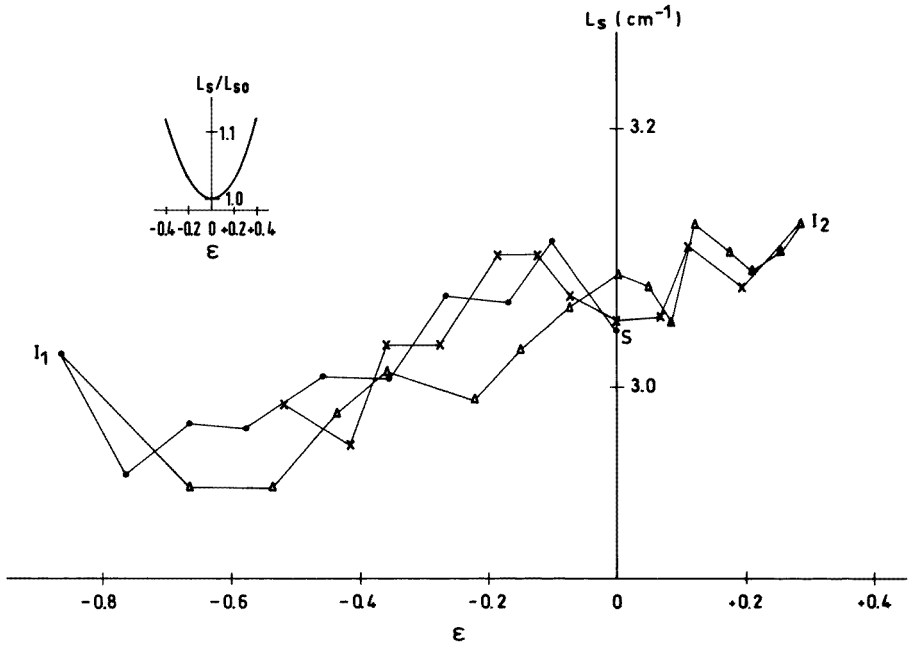

Figure 6. The total length, L_S, of films divided by the total area, as a function of strain, ε, in uniaxial deformation of foam sample 2. The foam, originally at S, was compressed to I_1, then extended to I_2 and finally compressed to $\varepsilon \simeq -0.5$. The inset is a plot of $L_S(\varepsilon)$ for homogeneous deformation of randomly oriented lines in an incompressible medium. Different symbols are used for the experimental points in different cycles.

where A is the total area of the foam sample and w is the width ($w\,\mathrm{d}\varepsilon = \mathrm{d}w$). When $F > 0$ the force is tensile and when $F < 0$ the force is compressive. Since L_S increases with ε, the force is always tensile (the confining bars attract each other).

The force F is the resultant of the contractile tension of the films connected to the bars (γ per film) and of the pressure forces acting on the bars. The pressure is larger on the side of the froth, the difference being approximately γ/r, where r is an average radius of curvature of the extreme films at a bar. If ℓ is the average bar length covered by one bubble, the total force F is:

$$F = \frac{L\gamma}{\ell}\left(1 - \frac{\ell}{r}\right) \tag{6}$$

where L is the length of each bar covered by the foam (L/ℓ is the number of bubbles contacting a bar). The sign of F depends on whether ℓ/r is larger or smaller than one. The average slope of $L_S(\varepsilon)$ in the plot of figure 6 gives $\ell/r \cong 0.9$, which is reasonable.

Deformation by simple stretching of the films would lead to a dependence of $\Delta L_S = L_S(\varepsilon) - L_S(0)$ on ε^2 for small ε, with $\Delta L_S = \frac{1}{2}(Y/\gamma)\varepsilon^2$; the Young's modulus Y is given by equation (1). For a honeycomb, the result is $\Delta L_S/L_S(0) = \varepsilon^2/8$. A parabolic dependence also arises in homogeneous deformation of a distribution of lines of random orientation, with $\Delta L_S/L_S(0) = \frac{3}{4}\varepsilon^2$, as shown in the appendix (see inset in figure 6). However, this result does not take into account the constraint of 120° triple junctions, that prevails in a slowly deforming liquid foam. The observed linear variation of L_S (foam energy) with ε is therefore a consequence of the deformation mechanism based on T1 events constrained by 120° triple junctions.

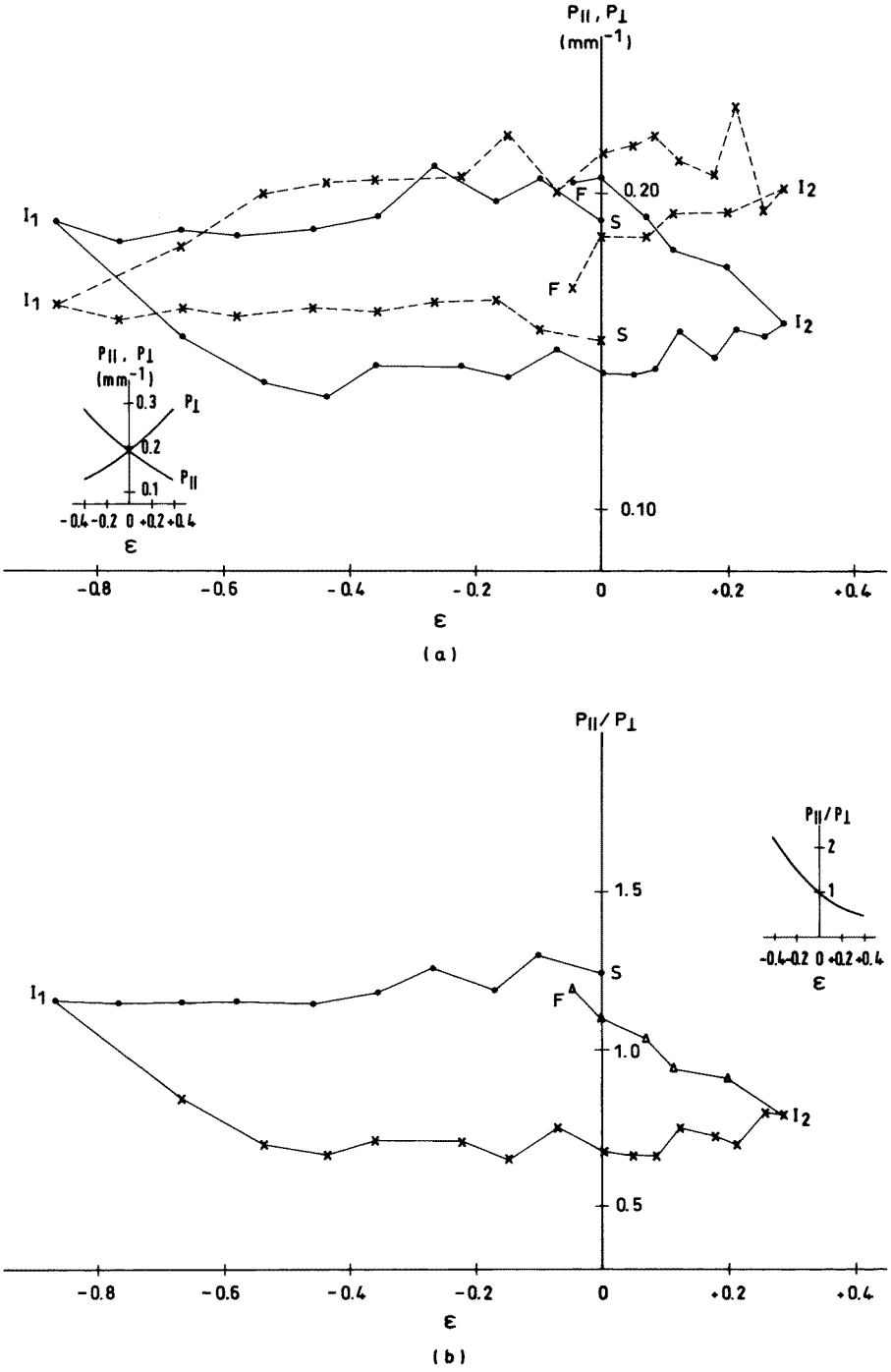

Figure 7. Evolution with strain, ε, of: (a) $P_\parallel$ (●) and $P_\perp$ (×) and (b) $P_\parallel/P_\perp$, for foam sample 2. $P_\parallel$ and $P_\perp$ are the numbers of films intersected per unit length of a family of straight lines, respectively parallel and perpendicular to the direction of the imposed strain. The insets show the evolution of $P_\parallel$, $P_\perp$ (calculated for the experimental $L_{S_0} = 3.04\,\mathrm{cm}^{-1}$) and $P_\parallel/P_\perp$ in homogeneous deformation of lines of initial random orientation in an incompressible medium.

3.6. Orientation of films

Figure 7(a) shows plots of the measured values of $P_\parallel$ and $P_\perp$, the number of film intersections per unit length of straight lines oriented parallel and perpendicular to the direction of bar displacement, respectively, as a function of ε in a deformation cycle of foam sample 2. Figure 7(b) is a plot of $P_\parallel/P_\perp$.

Initially $P_\parallel/P_\perp$ is slightly above one, in spite of the fact that the bars constrain the films to contact them at 90°, which would decrease $P_\parallel$ and $P_\perp$. In the first compression, $P_\parallel$ and $P_\perp$ change little with deformation. In subsequent tension, $P_\parallel$ decreases and $P_\perp$ increases more noticeably. There is, in general, a tendency for the films to orient parallel to the direction of elongation or, equivalently, for the bubbles to deform in the same way as their aggregate. This conclusion is confirmed by the plot of $P_\parallel/P_\perp$ in figure 7(b). Note that $P_\parallel/P_\perp$ does not return to the same value after a single cycle tension/compression.

The orientation effect observed is slight and much smaller than the re-orientation that would occur in homogeneous uniaxial deformation of a distribution of lines drawn on an incompressible medium (see the appendix). This is illustrated in the insets of figure 7.

4. Conclusions

Deformation of 2D monolayer liquid foams occurs essentially by neighbour switching events, both inside the foam (T1 events) and at the confining walls (T1′ events). No transitions of other types happened (e.g. associated with the liquid menisci [1]). The number of switchings per bubble was proportional to the strain ε and of the order of ε. For a given strain rate, $\dot{\varepsilon}$, the average time interval between two T1 events involving a given bubble is thus around $0.2/\dot{\varepsilon}$ (four bubbles are involved in a switching). The second moment of the distribution of the number of sides of the bubbles did not change by deformation, implying that the switching events do not occur at random edges, but rather at edges separating bubbles with many sides. The topological changes accompany metric changes. The total length of films (proportional to foam energy) increases in tension and decreases in compression, but the variation is small (small tensile forces). Films tend to reorient under deformation, but the effect is much smaller than the one that would result if deformation were homogeneous. Deformation scarcely affects the shape of the individual bubbles which rearrange as if they were nearly rigid. In this rearrangement, the bubbles nevertheless follow, in general, irregular trajectories that deviate from those for homogeneous deformation.

Appendix

In homogeneous deformation of a 2D incompressible medium, the coordinates x, y of a point initially at x_0, y_0 are:

$$\begin{aligned} y &= y_0\,\mathrm{e}^{\varepsilon} \\ x &= x_0\,\mathrm{e}^{-\varepsilon} \end{aligned} \tag{A1}$$

where ε is the strain ($\varepsilon = \ln y/y_0 = \ln w/w_0$); w is the width in the direction of the applied strain. $\varepsilon > 0$ represents elongation along the y axis.

The length of a short segment, $\mathrm{d}s_0$, at an angle θ_0 with the x axis, changes to:

$$\mathrm{d}s = \mathrm{d}s_0[\mathrm{e}^{-2\varepsilon}\cos^2\theta_0 + \mathrm{e}^{2\varepsilon}\sin^2\theta_0]^{1/2} \tag{A2}$$

while its inclination changes to θ, with

$$\tan\theta = \mathrm{e}^{2\varepsilon}\tan\theta_0. \tag{A3}$$

Consider a distribution of lines of length $\ell_S(\theta)\,\mathrm{d}\theta$ per unit area in the interval $\theta, \theta + \mathrm{d}\theta$. Assume that initially $l_S(\theta) = \ell_{S_0}$ is independent of θ. The initial total length per unit area is $L_{S_0} = \pi \ell_{S_0}$. After deformation the total length will be (equation (A2))

$$L_S = \ell_{S_0} \int_0^{\pi/2} [\mathrm{e}^{-2\varepsilon} \cos^2\theta_0 + \mathrm{e}^{2\varepsilon} \sin^2\theta_0]^{1/2}\,\mathrm{d}\theta_0. \tag{A4}$$

Note that $L_S(\varepsilon) = L_S(-\varepsilon)$. Equation (A4) can assume the form

$$\frac{L_S}{L_{S_0}} = \frac{2}{\pi}\,\mathrm{e}^{\varepsilon} \int_0^{\pi/2} [1 - (1 - \mathrm{e}^{-4\varepsilon}) \sin^2\alpha]^{1/2}\,\mathrm{d}\alpha \tag{A5}$$

which is a standard complete elliptic integral. In the inset of figure 6 is shown a plot of L_S/L_{S_0} as a function of ε.

The power series of L_S is

$$\frac{L_S}{L_{S_0}} = 1 + \frac{3}{4}\varepsilon^2 + \cdots. \tag{A6}$$

We obtain the number of intersections of lines per unit length of straight lines in a given direction by projecting the lines on that direction. Calculating $\cos\theta$ and $\sin\theta$ from equation (A3) as a function of θ_0 and ε we easily obtain

$$\begin{aligned} P_{\parallel} &= \frac{2L_{S_0}}{\pi}\,\mathrm{e}^{-\varepsilon} \\ P_{\perp} &= \frac{2L_{S_0}}{\pi}\,\mathrm{e}^{\varepsilon} \end{aligned} \tag{A7}$$

and

$$\frac{P_{\parallel}}{P_{\perp}} = \mathrm{e}^{-2\varepsilon}. \tag{A8}$$

The insets in figure 7 show plots of equations (A7) and (A8).

References

[1] Fortes M A and Rosa M E to be published
[2] Kraynik A M 1988 *Annu. Rev. Fluid Mech.* **20** 325
[3] Weaire D and Fortes M A 1994 *Adv. Phys.* **43** 685
[4] Weaire D, Bolton F, Herdtle T and Aref H 1992 *Phil. Mag. Lett.* **66** 293
[5] Hutzler S, Weaire D and Bolton H 1995 *Phil. Mag.* B **71** 277
[6] Durian D J 1997 *Phys. Rev.* E **55** 1739
[7] Yi Jiang 1998 *PhD Thesis* Notre Dame University, IN
[8] Gopal A D and Durian D J 1995 *Phys. Rev. Lett.* **75** 2610
[9] Rosa M E and Fortes M A 1998 *Phil. Mag.* A **77** 1423
[10] Kahn S A and Amstrong RC 1986 *J. Non-Newtonian Fluid Mech.* **22** 1
[11] Weaire D 1989 *Phil. Mag. Lett.* **60** 27
[12] Weaire D and Rivier N 1984 *Contemp. Phys.* **25** 59
[13] Rosa M E and Fortes M A 1999 *Phil. Mag.* A **79** 1871
[14] Okuzono T and Kawasaki K 1995 *Phys. Rev.* E **51** 1246
[15] Dennin M and Knobler C M 1997 *Phys. Rev. Lett.* **78** 2485
[16] Ashby M F and Verrall R A 1973 *Acta Metall.* **21** 149
[17] Vaz M F and Fortes M A 1997 *J. Phys.: Condens. Matter* **9** 8921
[18] Kawasaki K, Okuzono T, Kawakatsu T and Nagai T 1992 *Proc. Int. Workshop on Physics of Pattern Formation* ed S Kai (Singapore: World Scientific)
[19] Godrèche C, Kosov I and Yekuteli F 1992 *Phys. Rev. Lett.* **69** 2674
[20] Fradkov V E 1988 *Phil. Mag. Letters* **58** 271